RadioGraphics

Pretreatment Evaluation of Prostate Cancer: Role of MR Imaging and ^{1}H MR Spectroscopy[1]

CME FEATURE

See accompanying test at http://www.rsna.org/education/rg_cme.html

LEARNING OBJECTIVES FOR TEST 4

After reading this article and taking the test, the reader will be able to:

- Identify the MR imaging features of the normal prostate gland.
- Describe the MR imaging and MR spectroscopic imaging features of prostate cancer.
- Discuss the incremental value of MR imaging and MR spectroscopic imaging in the pretreatment work-up of prostate cancer.

Filip G. Claus, MD, PhD • Hedvig Hricak, MD, PhD • Robert R. Hattery, MD

Magnetic resonance (MR) imaging and hydrogen 1 MR spectroscopy of the prostate gland are performed during the same examination with a conventional clinical MR unit. Prostate zonal anatomy and prostate cancer are best depicted on multiplanar T2-weighted MR images. MR imaging and ^{1}H MR spectroscopy are not used as an initial diagnostic tool. Their use in tumor detection is reserved for patients with elevated prostate-specific antigen levels in whom previous biopsy results were negative. The use of MR imaging and ^{1}H MR spectroscopy for the evaluation of tumor location, local extent (extracapsular extension and/or seminal vesicle invasion), volume, and aggressiveness is generating strong clinical interest. In staging and treatment planning, MR imaging has been shown to have an incremental value additive to the value of clinical nomograms. Furthermore, anatomic and metabolic mapping of the prostate gland with ^{1}H MR spectroscopy offers the possibility of optimizing treatment planning (watchful waiting, surgery, or radiation therapy [intensity-modulated radiation therapy or brachytherapy]), thus further expanding the role of MR imaging in the achievement of patient-specific, individualized treatment.

Abbreviation: PSA = prostate-specific antigen

Index terms: Neoplasms, staging, 844.1214, 844.12145 • Prostate neoplasms, MR, 844.1214, 844.12145

RadioGraphics 2004; 24:S167–S180 • **Published online** 10.1148/24si045516 • **Content Codes:** GU MR

[1]From the Department of Radiology, Memorial Sloan-Kettering Cancer Center, 1275 York Ave, C278, New York, NY 10021 (F.G.C., H.H.); and Department of Diagnostic Radiology, University of Arizona, Tucson (R.R.H.). Received March 30, 2004; revision requested April 19; revision received May 5 and accepted May 11. All authors have no financial relationships to disclose. Supported by National Institutes of Health grant R01 CA76423. **Address correspondence to** F.G.C. (e-mail: *clausf@mskcc.org*).

Introduction

Prostate cancer is the most common cancer and the second leading cause of cancer death in American men. The American Cancer Society estimates that in 2004, 230,110 new cases of prostate cancer will be diagnosed in the United States and 29,900 people will die of the disease, increases of 4.5% and 3.5%, respectively, compared with 2003 data (1). Because of the advent of prostate-specific antigen (PSA) screening, most prostate cancers are now diagnosed at an earlier stage. At present, 86% of newly diagnosed prostate cancers are localized within the gland and patients have a 5-year relative (ie, adjusted for life expectancy) survival rate of 100%. The 5-year relative survival rate for all stages of prostate cancer is 98%, which indicates that prostate tumors have a slow growth rate and allow for prolonged survival, even in patients with metastases at diagnosis (2,3).

Controversy exists with regard to the appropriate management of prostate cancer. The choice of treatment depends on the patient's age at diagnosis, the stage and aggressiveness of the tumor, the potential side effects of the treatment, and patient comorbidity (4–6). The most common treatment side effects are erectile dysfunction and urinary incontinence. Efforts to reduce treatment morbidity while maximizing treatment effects have led to the demand for patient-specific and disease-targeted therapies. Although there are a number of clinical parameters and clinical nomograms to help with the choice of treatment, there is a growing demand for further individualization of treatment plans (3,7). For all clinical nomograms, the highest priority is the differentiation between indolent and aggressive disease. The major indicator of tumor aggressiveness is the Gleason grade. A biopsy-determined Gleason grade, although valuable, is subject to sampling error. It has been reported that after radical prostatectomy the biopsy-determined Gleason grade is increased in as many as 54% of patients (8). Furthermore, prostate cancer is histologically heterogeneous and multifocal in as many as 85% of patients. Thus, a technique that noninvasively demonstrates the presence, extent, and aggressiveness of prostate cancer could make a substantial contribution to the decision-making process for individualized treatment. Magnetic resonance (MR) imaging and proton MR spectroscopy (hydrogen 1 MR spectroscopy) enable the noninvasive evaluation of anatomic and biologic tumor features and, thus, may play an important role in the detection, localization, and staging of prostate cancer and help guide treatment selection and planning (9).

This article addresses the advantages, limitations, and need for critical evaluation of endorectal MR imaging and proton MR spectroscopy in the diagnostic evaluation of prostate cancer. Key findings of zonal anatomy and spectroscopic features of the normal prostate gland are discussed. Our objective is to illustrate the potential incremental value of MR imaging and MR spectroscopy in the diagnostic work-up of prostate cancer, with emphasis on tumor localization, metabolic interrogation, and staging. We include examples to illustrate the key MR imaging features used to detect prostate cancer and determine local extent, and we discuss the role of MR imaging and MR spectroscopy in treatment planning.

MR Imaging and MR Spectroscopic Imaging Techniques

Although the "optimal" choice of equipment (specifically, magnet strength) and imaging sequences are always dependent on the instruments available, in this section we present general guidelines for diagnostic image and spectral quality. Because a combination of MR imaging and spectroscopy is desirable, a magnetic field strength of at least 1.5 T is required. The combined use of endorectal and pelvic phased-array coils and the generation of faster imaging sequences are recommended. Although imaging parameters are dependent on the type of imaging unit used and the field strength, in general the following imaging sequences are recommended: *(a)* T1-weighted axial imaging of the pelvic region is used for detecting nodal disease and postbiopsy intraglandular hemorrhage, and *(b)* thin-section T2-weighted imaging with a smaller field of view (~14 cm) in

the axial, sagittal, and coronal planes is used for tumor detection, localization, and staging. The use of dynamic contrast material–enhanced MR imaging is optional (10,11).

To avoid under- and overestimation of tumor location and extent, MR imaging should be delayed for at least 4–6 weeks after prostate biopsy (12,13).

A number of different ^{1}H MR spectroscopic techniques have been described. At present, the commercially available spectroscopic imaging techniques include chemical shift imaging (14) with point-resolved spectroscopy, voxel excitation, and band-selective inversion with gradient dephasing for water and lipid suppression (15). Chemical shift imaging refers to the multivoxel technique that enables the acquisition of voxels in single or multiple sections. With point-resolved spectroscopy, a cubic or rectangular voxel is generated by acquiring three orthogonal section-selective pulses, that is, a 90° pulse followed by two 180° pulses. The setup for spectroscopic imaging is the same as that for morphologic imaging, and both datasets are usually acquired in the same examination to overlay metabolic information directly on the corresponding anatomic images. The combined MR imaging–MR spectroscopic examination takes approximately 1 hour.

Prostate Gland Anatomy

Familiarity with the normal anatomy of the prostate gland is crucial for image interpretation. MR imaging depicts the zonal anatomy of the prostate with exquisite detail because of its high spatial resolution, superior contrast resolution, multiplanar capability, and large field of view. The prostate is histologically composed of glandular (acinar) and nonglandular elements. The major nonglandular elements are the prostatic urethra and the anterior fibromuscular band. The glandular prostate consists of outer and inner components, which are differentiated by location, duct anatomy, and histologic characteristics. The inner prostate consists of the periurethral glandular tissue and the transition zone, whereas the outer prostate consists of the central and peripheral zones.

The periurethral glands compose less than 1% of the glandular prostate. The transition zone constitutes only about 5% of the glandular prostate in young men. The central zone forms most of the glandular tissue of the prostatic base and makes up about 25% of the glandular prostate. The peripheral zone is the major glandular component of the prostate, composing 70% of the prostate in healthy young men. The junction of the transition and peripheral zones is marked by a visible linear boundary, which is often referred to as the prostate pseudocapsule or surgical capsule. The true prostate capsule surrounds the peripheral zone. The neurovascular bundles are seen posterolateral to the prostate capsule.

Although the zones of the prostate gland were first described in the 1960s, the terms were not commonly used in clinical practice until the 1980s (16). The zones are not only defined histologically; many prostatic diseases have a zonal distribution. For example, 70% of adenocarcinomas arise in the peripheral zone, 20% in the transition zone, and 10% in the central zone. Conversely, benign prostatic hyperplasia usually involves the transition zone. This zone, which is small and inconsequential in young men, becomes hyperplastic and progressively larger with age. In the radiology literature, the terms *central gland* (which refers collectively to the periurethral, central, and transition zones) and *peripheral gland* (which includes only the peripheral zone) are used as well, especially when describing the sonographic appearance of the prostate zonal anatomy.

Other terms used frequently in clinical practice are those describing the anatomic division of the prostate into sextants. The sextant description of the prostate refers to the systematic biopsy of the right and left base, mid-gland, and apex of the prostate gland.

MR Imaging Appearance of Normal Prostate Anatomy

On T1-weighted MR images, the normal prostate gland demonstrates homogeneous intermediate-to-low signal intensity. As with computed tomography (CT), T1-weighted MR imaging has insufficient soft-tissue contrast resolution for visualizing the intraprostatic anatomy or abnormality.

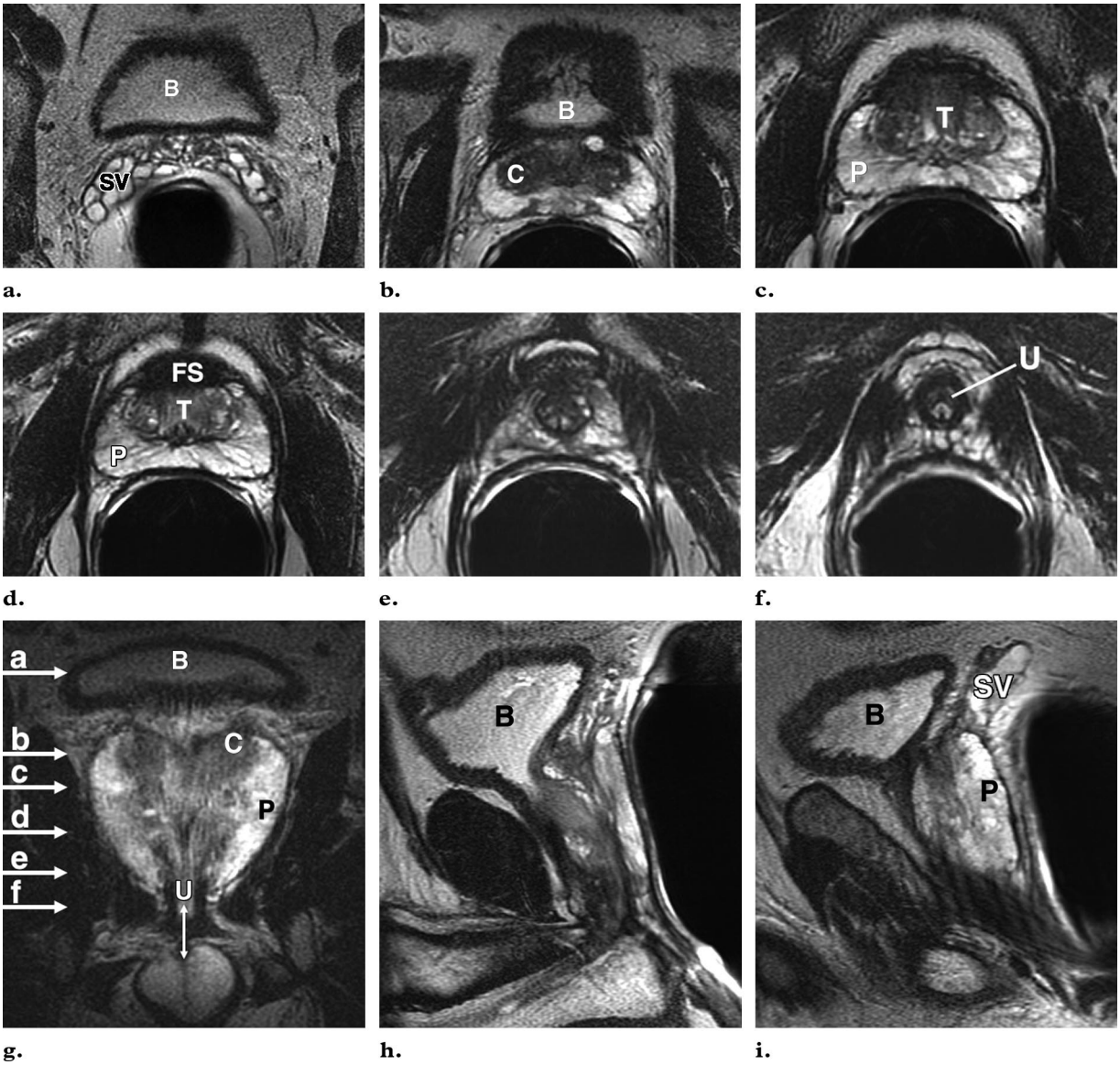

Figure 1. Normal prostate zonal anatomy in a 60-year-old man depicted with T2-weighted axial MR images obtained at the level of the seminal vesicles **(a)**, the base of the prostate **(b)**, the mid-gland **(c, d)**, the apex **(e)**, and the membranous urethra **(f)**, as well as coronal **(g)**, midsagittal **(h)**, and parasagittal **(i)** MR images. The letters in **g** correspond to the anatomic levels used for images **a–f**. The vertical line in **g** indicates the membranous urethral length. *B* = urinary bladder, *C* = central zone, *FS* = anterior fibromuscular stroma, *P* = peripheral zone, *SV* = seminal vesicles, *T* = transition zone, *U* = urethra.

The zonal anatomy of the prostate gland is best depicted on high-resolution T2-weighted images (Fig 1).

On T2-weighted images (Fig 1), the normal peripheral zone demonstrates a high signal intensity. The peripheral zone is surrounded by a thin rim of low signal intensity, which represents the anatomic or true capsule. Low-signal-intensity foci posterolateral to the capsule are indicative of neurovascular bundles. The signal intensities in

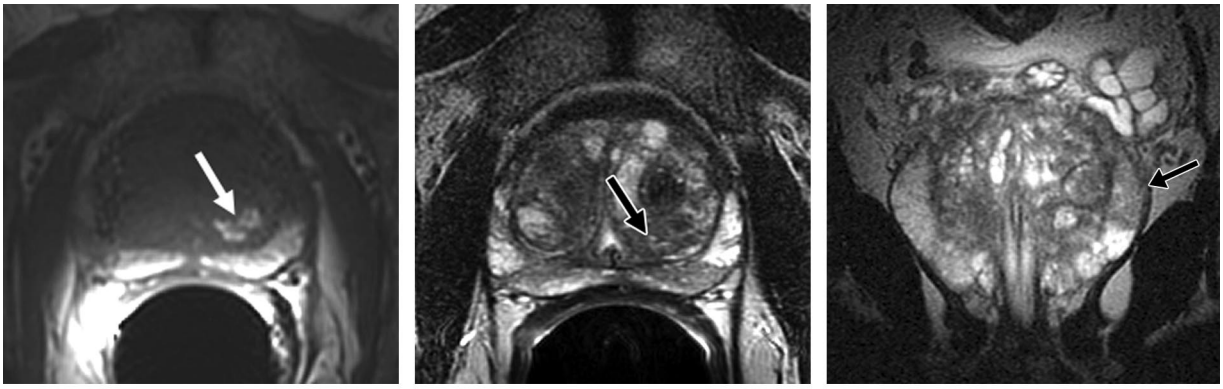

a. b. c.

Figure 2. Postbiopsy hemorrhage. T1- **(a)** and T2- **(b)** weighted axial MR images and T2-weighted coronal MR image **(c)** demonstrate extensive bilateral postbiopsy hemorrhage in the peripheral zones. The transition zone in the left lobe demonstrates high signal intensity on the T1-weighted image (arrow in **a**) and low signal intensity on the T2-weighted images (arrow in **b** and **c**).

the central and transition zones are lower than those in the peripheral zone. The central and transition zones have similar signal intensities and are best differentiated by their respective anatomic locations. The anterior fibromuscular stroma has low signal intensity. The proximal urethra is rarely identifiable unless a Foley catheter is present or a transurethral resection has been performed. The distal prostatic urethra can be seen as a low-signal-intensity ring in the lower prostate. The vas deferens and seminal vesicles demonstrate high signal intensity.

On contrast-enhanced MR images, the peripheral zone enhances more than the transition or central zone. The contrast resolution is similar to that seen on T2-weighted images.

MR Imaging Appearance of Prostate Cancer

On T2-weighted images, prostate cancer usually demonstrates low signal intensity in contrast to the high signal intensity of the normal peripheral zone. Low signal intensity in the peripheral zone, however, can also be seen in several benign conditions, such as hemorrhage, prostatitis, hyperplastic nodules, or posttreatment sequelae (eg, as a result of irradiation or hormonal treatment) (Fig 2).

Dynamic contrast-enhanced MR imaging was developed to help achieve a higher accuracy in prostate cancer localization and staging than that obtained with conventional T2-weighted MR imaging. The rationale for dynamic contrast-enhanced MR imaging is the expectation that increased microvascular density in prostate cancer would result in different contrast enhancement than that seen in normal tissue. Numerous contrast enhancement parameters can be used to differentiate cancerous from benign tissue, including onset time, time to peak enhancement, peak enhancement, relative peak enhancement, and washout time. Results of a recent study suggest that the peak enhancement of cancer relative to that of surrounding benign tissue is the most accurate parameter for cancer localization (17). An alternative to parameter calculation is to detect cancer as areas of enhancement on early postcontrast images (within the first 30–60 seconds after contrast material injection) (18). The optimal balance between temporal and spatial resolution is still controversial. Results of a meta-analysis (19) indicated that dynamic contrast-enhanced MR imaging can help improve the accuracy of prostate cancer staging; however, only eight studies were used in the analysis. In summary, although the early experience with dynamic contrast-enhanced MR imaging in the evaluation of prostate cancer seems promising, more studies are necessary to optimize the technology and make a more definitive judgment about its clinical value.

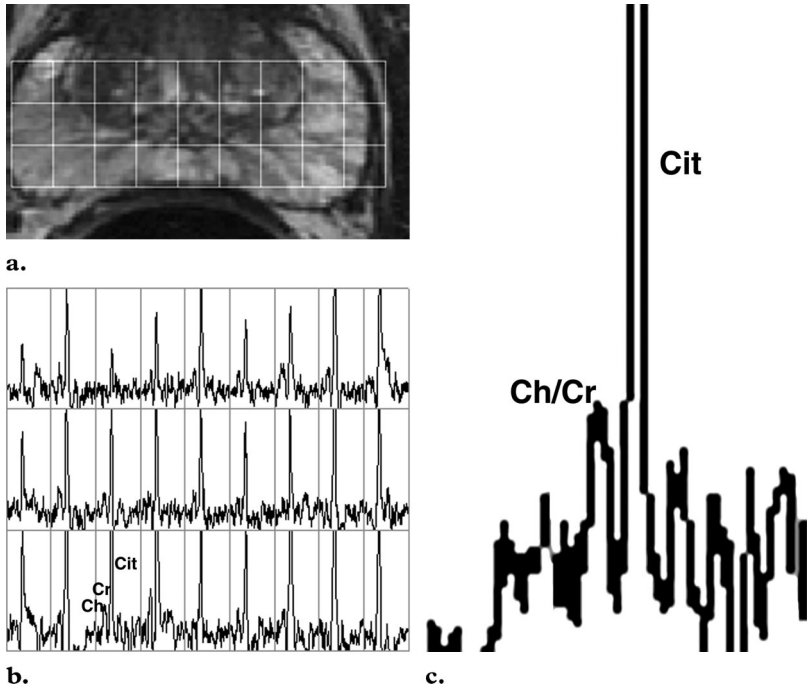

Figure 3. Normal prostate gland depicted with T2-weighted axial MR image **(a)** and spectra obtained with ^{1}H MR spectroscopy **(b, c)**. The spectra grid for the cellular metabolites citrate *(Cit)*, choline *(Ch)*, and creatine *(Cr)* shown in **b** corresponds to the grid overlaid on the T2-weighted axial image.

MR Spectroscopy of the Prostate Gland

MR spectroscopy provides metabolic information about prostatic tissue by displaying the relative concentrations of chemical compounds within contiguous small volumes of interest (voxels). Currently, three-dimensional proton MR spectroscopic metabolic mapping of the entire gland is possible with a resolution of 0.24 mL. Proton MR spectroscopy displays concentrations of citrate, creatine, and choline. Normal prostate tissue contains high levels of citrate (higher in the peripheral zone than in the central and transition zones). Glandular hyperplastic nodules, however, can demonstrate citrate levels as high as those observed in the peripheral zone. In the presence of prostate cancer, the citrate level is diminished or undetectable because of a conversion from citrate-producing to citrate-oxidating metabolism. The choline level is elevated owing to a high phospholipid cell membrane turnover in the proliferating malignant tissue. Hence, the method for depicting tumors is based on an increased choline-citrate ratio. Because the creatine peak is very close to the choline peak in the spectral trace, the two may be inseparable; therefore, for practical purposes, the ratio of choline and creatine to citrate is used for spectral analysis in the clinical setting (Fig 3).

There is no consensus about spectral interpretation. The classification system described by Kurhanewicz et al (20) is often used. In that system, a voxel is classified as normal, suspicious for cancer, or very suspicious for cancer. Furthermore, a voxel may contain nondiagnostic levels of metabolites or artifacts that obscure the metabolite frequency range. Voxels are considered suspicious for cancer if the ratio of choline and creatine to citrate is at least 2 standard deviations (SDs) higher than the average ratio for the normal peripheral zone. Voxels are considered very suspicious for cancer if the ratio of choline and creatine to citrate is higher than 3 SDs above the average ratio (21) (Fig 4). Voxels considered nondiagnostic contain no metabolites with signal-to-noise ratios greater than 5. In voxels in which only one metabolite is detectable, the other metabolites are assigned a value equivalent to the SD of noise. MR spectroscopy enables analysis of the metabolism in the entire prostate gland. Combined with MR imaging, proton MR spectroscopy has shown excellent sensitivity and specificity in the detection of cancer in the peripheral zone of the prostate (22).

Prostate Cancer Detection

Although routine screening for prostate cancer remains controversial, PSA testing is widely used in the United States. On the basis of data from the 2001 Behavioral Risk Factor Surveillance System (23), 57% of men at least 50 years of age underwent annual PSA testing, and 75% of all men in this age group reported being tested at least

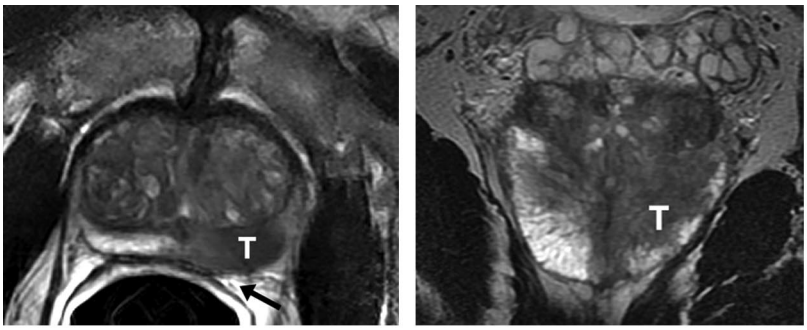

a. b.

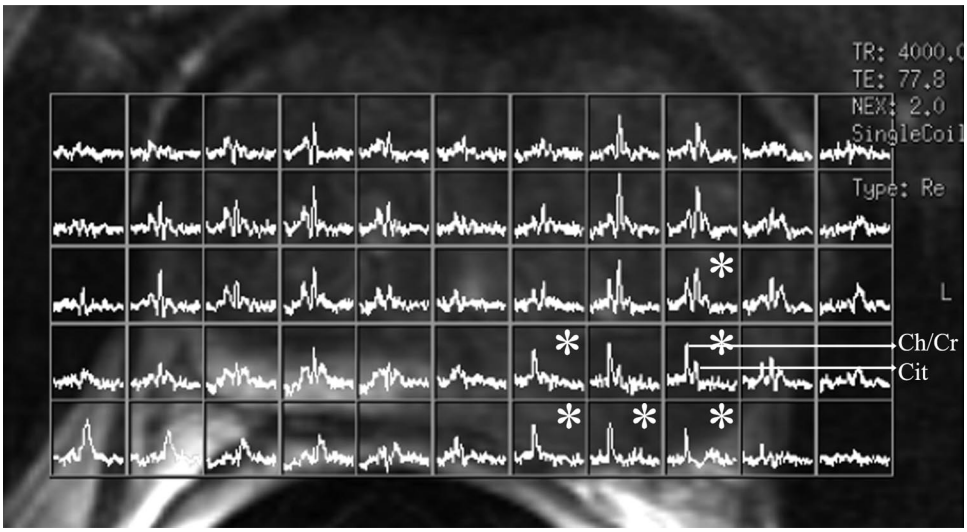

c.

Figure 4. Biopsy-proved Gleason grade 8 adenocarcinoma in a 71-year-old man with a PSA level of 5.65 ng/mL. **(a, b)** T2-weighted axial MR image **(a)** and T2-weighted coronal MR image **(b)** show that the dominant tumor (*T*) within the left peripheral zone extends from the apex to the base. Obliteration of the left rectoprostatic angle (arrow in **a**) is indicative of extracapsular extension. **(c)** On the spectra from ^{1}H MR spectroscopy, voxels marked with ∗ show an increase in choline *(Ch/Cr)* and a marked decrease in or absence of citrate *(Cit);* these voxels correspond to the low-signal-intensity region on the axial MR image **(a)**. The metabolic profile is indicative of a high-grade tumor. Findings at surgery and histopathologic examination helped confirm a large Gleason grade 8 tumor with extracapsular extension (stage T3a).

once. A traditional threshold for recommending prostate biopsy is a PSA level greater than 4 ng/mL. Measurements such as PSA velocity, PSA density, and free PSA are sometimes used to improve the accuracy of the test. Causes of elevated PSA levels aside from cancer include biopsy of the prostate gland, transurethral prostatectomy, acute urinary retention, subclinical prostatic inflammation, acute prostatitis, and benign prostatic hyperplasia. Stage distribution is affected substantially by PSA testing, and most of the cases (up to 70%) are diagnosed in the absence of symptoms (24). The digital rectal examination is another common screening test. Ultrasonography (US) is recommended only if the results of either PSA testing or digital rectal examination are abnormal and suspicious for cancer. Needle biopsy, with or without transrectal US guidance, is the method most commonly used for making the histologic diagnosis of prostate cancer. MR imaging and/or MR spectroscopy are not used as a first approach to diagnose prostate cancer but may be useful for targeted biopsy, especially in patients with PSA levels indicative of cancer but negative results from previous biopsies; this situation occurs most commonly with lesions in the anterior peripheral or transition zone (ie, regions not palpable at digital rectal examination and often not routinely sampled or targeted during biopsy) (25,26).

Prostate Cancer Diagnosis and Characterization

Prostate cancer is a multifocal and histologically heterogeneous disease, and biopsy is limited in defining all cancer sites and grades. Estimates suggest that with a threshold PSA value of 4.1 ng/mL, 82% of cancers in men younger than 60 years and 65% of cancers in men older than 60 years could be missed (27). Biopsy is considered the preferred method for prostate cancer detection and characterization; however, when biopsy results were compared with those from radical prostatectomy for sextant tumor localization, the positive predictive value of biopsy was 83.3% and the negative predictive value 36.4% (28). In other studies, up to 30% of cancers were missed at sextant biopsy (29), and the technique was not accurate for defining the location and extent of prostatic carcinoma (30).

One of the most challenging characteristics of prostate cancer is its variability in biologic aggressiveness. In addition, biopsy specimens are not accurate in the prediction of Gleason score. Studies of 226 and 449 patients (8,31) found that biopsy enabled the correct prediction of radical prostatectomy Gleason grade in 31% and 58% of cases, respectively. Therefore, the need to improve both tumor detection and assessment of tumor aggressiveness is compelling.

The combined use of MR imaging and MR spectroscopy improves detection of tumors within the peripheral zone (21,22,30). It has also been shown to increase the specificity in the localization of prostate cancer in the peripheral zone, although with moderate interreader agreement (22). Preliminary reports of MR spectroscopy assessment of tumor aggressiveness have shown promise. The ratio of choline and creatine to citrate in the lesion shows correlation with the Gleason grade, with the elevation of choline and reduction of citrate indicative of increased cancer aggressiveness (32).

It has also been shown that metabolic and volumetric data obtained with MR spectroscopy correlate with the Gleason grade at pathologic examination (32). It has been recommended that the maximum ratio of choline and creatine to citrate combined with tumor volume at MR spectroscopy be used as an index to help predict tumor aggressiveness (25). Because Gleason grade is an important predictor of patient outcome, this finding provides a rationale for adding MR imaging and/or MR spectroscopy to the pretreatment evaluation of patients with prostate cancer. To expand on the current single-institution results, a multicenter trial is being undertaken to investigate the role of MR imaging alone and in combination with MR spectroscopy in the detection and characterization of prostate cancer. This trial includes an evaluation of the incremental value of MR imaging and MR spectroscopy combined in the diagnostic work-up for prostate cancer (33).

Prostate Cancer Staging

Historically, the stage of prostate cancer was based on the Jewett classification; only in the past 10 years has the TNM system prevailed. At present, however, both staging systems are in common use. The Jewett classification system (stages A–D) was described in 1975 and has since been modified. In 1997, the American Joint Committee on Cancer and the International Union Against Cancer adopted a revised TNM system that uses the same broad T stage categories as in the Jewett system but includes subcategories of T stage, including a stage to describe disease diagnosed by means of PSA screening. In 2002, the American Joint Committee on Cancer further revised the TNM classification system (34). This revised TNM system, as shown in Table 1, is clinically useful and more precisely stratifies newly diagnosed cancer.

Clinical T staging is largely dependent on imaging findings. Compared with CT, US, and digital rectal examination, MR imaging has a higher accuracy in the assessment of uni- or bilobar disease (stage T2), extracapsular extension and seminal vesicle invasion (stage T3), and invasion of adjacent structures (stage T4). The literature, however, shows a wide range (50%–92%) in the accuracy of local staging with MR imaging (19). Despite its high specificity in the identification of

Table 1
TNM System for Staging Prostate Cancer

Stage	Definition
Primary tumor	
TX	Primary tumor cannot be assessed
T0	No evidence of primary tumor
T1	Clinically, the tumor is neither palpable nor visible with imaging
T1a	Tumor is an incidental histologic finding in 5% or less of tissue resected
T1b	Tumor is an incidental histologic finding in more than 5% of tissue resected
T1c	Tumor identified with needle biopsy (eg, because of an elevated PSA level)
T2	Tumor confined within the prostate
T2a	Tumor involves one-half of one lobe or less
T2b	Tumor involves more than one-half of one lobe but not both lobes
T2c	Tumor involves both lobes
T3	Tumor extends through the prostate capsule
T3a	Extracapsular extension (unilateral or bilateral)
T3b	Tumor invades seminal vesicle(s)
T4	Tumor is fixed or invades adjacent structures other than seminal vesicles: bladder neck, external sphincter, rectum, levator muscles, and/or pelvic wall
Regional lymph nodes	
NX	Regional lymph nodes were not assessed
N0	No regional lymph node metastasis
N1	Metastasis in regional lymph node(s)
Distant metastasis	
MX	Distant metastasis cannot be assessed (not evaluated with any modality)
M0	No distant metastasis
M1	Distant metastasis
M1a	Nonregional lymph node(s)
M1b	Bone(s)
M1c	Other site(s) with or without bone disease

Source.—Reference 32.

Table 2
Extracapsular Extension Criteria on MR Images

Neurovascular bundle asymmetry
Tumor envelopment of the neurovascular bundle
Angulated contour of the prostate gland
Irregular, spiculated margin
Obliteration of the rectoprostatic angle

organ-confined disease and extracapsular extension, owing to lower sensitivity and substantial interobserver variability, the routine use of MR imaging in the local staging of prostate cancer remains controversial.

Increased experience in interpretation and a better understanding of morphologic criteria used to diagnose extraprostatic disease are key to further improving the role and accuracy of MR imaging in staging. The combined use of MR imaging and MR spectroscopy substantially improves the evaluation of extracapsular extension and decreases interobserver variability (22). In addition, the combined MR imaging–MR spectroscopy approach enables the assessment of tumor aggressiveness. Findings used to diagnose extracapsular extension at endorectal coil MR imaging are listed in Table 2 and illustrated in Figures 4, 5, and 6.

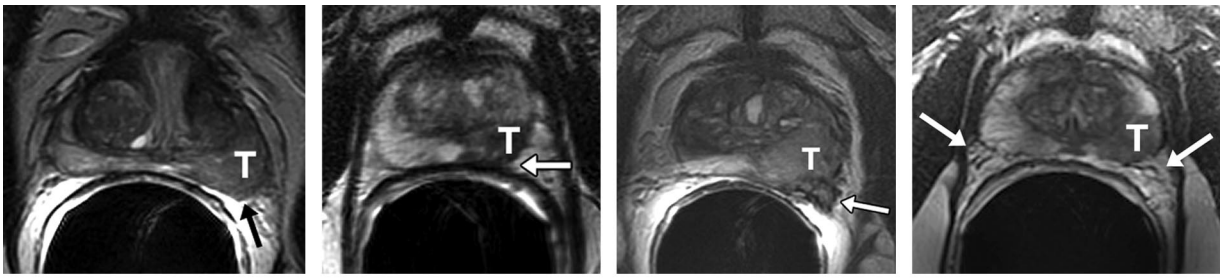

a. b. c. d.

Figure 5. Four different prostate cancer cases with extracapsular extension of the tumor *(T)*. T2-weighted axial MR images show an asymmetric bulge and spiculated margin (arrow in **a**), obliteration of the rectoprostatic angle (arrow in **b**), breach of the capsule with direct tumor extension and envelopment of the neurovascular bundle (arrow in **c**), and asymmetry of the neurovascular bundles (arrows in **d**).

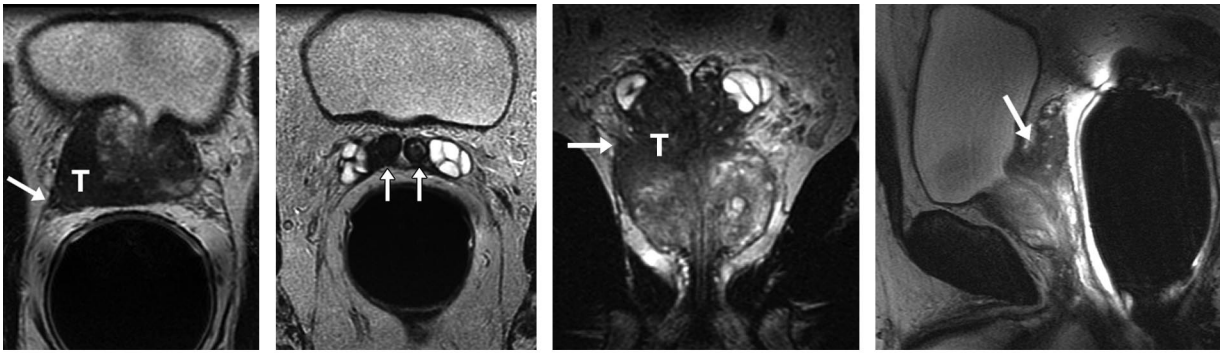

a. b. c. d.

Figure 6. Biopsy-proved adenocarcinoma in a 61-year-old man. **(a, b)** T2-weighted axial MR images obtained at the level of the base of the prostate **(a)** and at the seminal vesicles **(b)** show a low-signal-intensity tumor *(T)* in the base of the right lobe with extracapsular extension (arrow in **a**) and invasion into the seminal vesicles bilaterally (arrows in **b**). **(c)** T2-weighted coronal image shows asymmetry of the right and left lateral aspects of the base, with an angulated contour of the right base (arrow), a finding that is highly suggestive of extracapsular extension of the tumor *(T)*. **(d)** On the T2-weighted sagittal MR image, the fat plane between the seminal vesicle and the posterior urinary bladder is obliterated (arrow). The angle made by the posterior bladder wall and the anterior border of the seminal vesicles is more convex than that seen in healthy men (cf Fig 1i).

In addition to extracapsular extension, seminal vesicle invasion is an important prognostic clinical parameter because it is associated with the highest rates of treatment failure—second only to lymph node metastases (35,36). The combination of images obtained in the transaxial, coronal, and sagittal planes facilitates the diagnosis of both extracapsular extension and seminal vesicle invasion. The criteria for diagnosing seminal vesicle invasion at MR imaging are listed in Table 3.

MR imaging is also helpful for diagnosing the invasion of adjacent organs (eg, the urinary bladder and rectum). The sagittal imaging plane optimizes the evaluation of tumor extension into the bladder and rectum (Figs 7, 8).

In the evaluation of lymph node metastases, efficacy data for MR imaging and CT are similar, with both modalities having low sensitivity. Results of a recent investigation (37) showed that high-resolution MR imaging with lymphotropic superparamagnetic nanoparticles holds considerable promise in the detection of occult lymph node metastases. Radionuclide bone scanning is the initial imaging modality recommended for detecting bone metastases. Although MR imaging is more sensitive than radionuclide scanning, evaluation of the entire skeletal system has not been critically analyzed. Reported cutoff values of PSA level used to identify patients at high risk for lymph node and bone metastases are around 15 ng/mL and 20 ng/mL, respectively; however, there is considerable variation in cutoff values among different series in the literature (38,39).

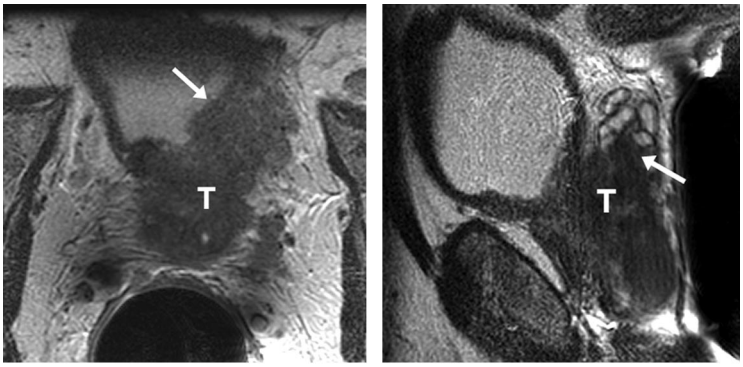

a. b.

Figure 7. Biopsy-proved Gleason grade 8 adenocarcinoma in a 58-year-old man with a PSA level of 50.0 ng/mL. T2-weighted axial **(a)** and sagittal **(b)** MR images reveal a large tumor *(T)* that invades the entire prostate gland and demonstrate gross extracapsular extension and direct invasion of the urinary bladder (arrow in **a**) and seminal vesicles (arrow in **b**).

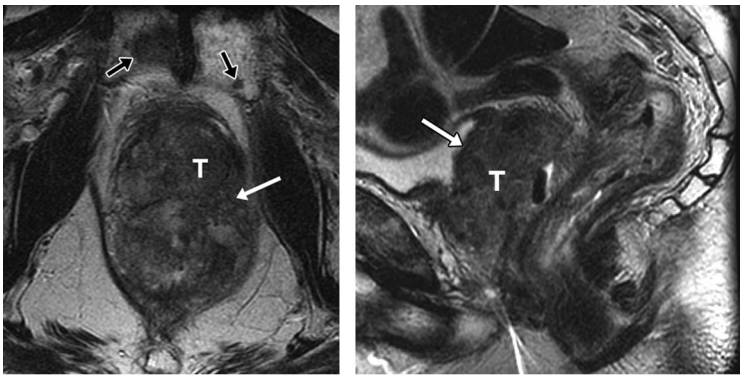

a. b.

Figure 8. Biopsy-proved Gleason grade 7 adenocarcinoma in a 62-year-old man with a PSA level of 15.1 ng/mL. T2-weighted axial **(a)** and sagittal **(b)** MR images demonstrate diffuse tumor invasion of the prostate gland with direct tumor *(T)* extension to the wall of the urinary bladder and the anterior rectal wall (white arrow). The multiple low-signal-intensity lesions (black arrows in **a**) in the pubic bones are consistent with bone metastases.

Table 3
Seminal Vesicle Invasion Criteria on MR Images

Focal low signal intensity of the seminal vesicle
Enlargement with a low-signal-intensity mass
Direct tumor extension from the base to the undersurface of the seminal vesicle
Expanded low-signal-intensity ejaculatory duct with low-signal-intensity seminal vesicle

Prostate Cancer Treatment Planning

The thrust of cancer care is risk-adjusted, patient-specific therapy designed to maximize cancer control while minimizing the risks of complications. Risk-adjusted, patient-specific treatment of prostate cancer necessitates the accurate characterization of the location and extent of cancer. The optimal therapeutic approach varies widely; options include watchful waiting, androgen ablation (chemical or surgical castration), hormone therapy, radical surgery, and various forms of radiation therapy (brachytherapy, external beam irradiation). The optimal treatment for prostate cancer is best selected on the basis of clinical TNM stage, Gleason grade, and the level of the circulating tumor marker, PSA. The decision to treat should also take into account patient age, disease stage, associated medical illnesses, and the patient's personal preferences. The inclusion of MR imaging and/or MR spectroscopic findings in clinical nomograms helps improve the prediction of cancer extent, thereby improving patient selection for local therapy. Other advantages of improved cancer staging include a better stratification of patients in clinical trials, the possibility of monitoring the progress of patients who select watchful waiting or other minimally aggressive cancer management options, and the guidance and assessment of emerging local prostate cancer therapies. MR spectroscopy has shown great promise in the differentiation of indolent from aggressive disease. Therefore, MR imaging and MR spectroscopy together have the potential to contribute to both the choice of treatment and treatment planning.

Surgery

Most cancers treated today are not palpable, and apart from the information obtained with US and biopsy, the surgeon has limited information about the size, location, and extent of the cancer. MR imaging can help refine the surgical plan, thus maximizing the preservation of periprostatic tissues (important for the recovery of urinary and sexual function) and minimizing the risk of positive surgical margins. The use of endorectal coil MR imaging before radical prostatectomy can have an influence on the surgical decision to spare or resect the neurovascular bundles; this is especially valuable in high-risk patient groups. MR imaging can also be useful for predicting intraoperative blood loss during radical retropubic prostatectomy (ie, a cutoff value of 4-mm separation from tumor to apical periprostatic veins at MR imaging has been shown to correlate with greater blood loss) (40). In addition, MR imaging can help predict urinary incontinence after radical retropubic prostatectomy. In a series of 211 patients, Coakley et al (41) demonstrated that the membranous urethral length, as measured at MR imaging, is associated with the return of urinary continence after surgery. Patients with a longer membranous urethra regain urinary continence at a substantially faster rate.

Radiation Therapy

The most commonly used forms of radiation therapy for prostate cancer are brachytherapy, three-dimensional conformal radiation therapy, and intensity-modulated radiation therapy. The guidelines for the optimal choice of treatment are not well established, and the choices are often empirical. The results of several retrospective analyses and the early results of clinical trials indicate that an increased radiation dose is associated with reduced rates of biochemical failure and may, therefore, increase local control rates and decrease the risk for distant metastasis and the rate of overall mortality (42–44). This observation is important in the treatment of intermediate- or high-risk prostate cancer patients; however, increased radiation doses may be associated with a risk of treatment morbidity (45). Both three-dimensional conformal radiation therapy and, in particular, intensity-modulated radiation therapy offer the possibility of combining very high radiation doses in areas of high tumor-cell density within the prostate gland without substantially increasing the risk of normal tissue damage. Because of its ability to show tumor location and extent, MR imaging can be of tremendous help in three-dimensional conformal or intensity-modulated radiation therapy planning, both of which require knowledge of tumor location, volume, and extent (Fig 9).

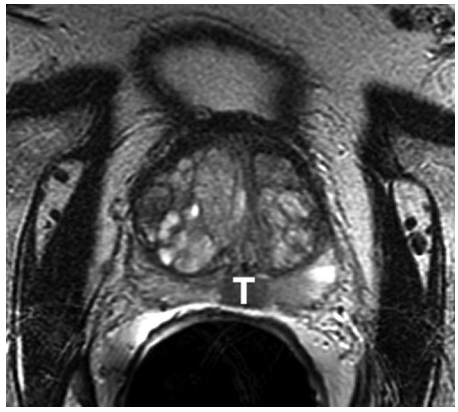

Figure 9. Biopsy-proved Gleason grade 8 adenocarcinoma in a 74-year-old man with a PSA level of 20.2 ng/mL. T2-weighted axial MR image shows a midline low-signal-intensity lesion in the peripheral zone with focal smooth bulging of the capsule. The patient was treated with intensity-modulated radiation therapy. The MR imaging findings, in particular the close spatial relationship between the tumor *(T)* and rectal wall, were helpful for designing the radiation treatment plan.

Further implementation of these technologic advances has increased the interest in imaging techniques that are able to help map tumor volume or localize more aggressive regions within the tumor, such as highly proliferating or hypoxic foci (46). Such imaging-optimized dose delivery has shifted radiation therapy planning toward a more individualized treatment approach. MR imaging is more accurate than CT in defining the prostate volume, with the highest nonagreement in the apex and posterior parts of the gland and the seminal vesicles (47–49). Prostate volumes derived with CT are larger than those derived with MR imaging. MR imaging is also more accurate in the anatomic delineation of surrounding structures, such as the rectal wall, the sigmoid, the urethra, and the penile bulb, which are at risk for radiation-induced tissue damage. The dose delivered to the rectal wall and bulb of the penis is substantially reduced with treatment plans based on the MR imaging–delineated prostate anatomy

compared with treatment plans based on the CT-delineated prostate anatomy, decreasing the risk of rectal and urologic complications (50). Metabolic mapping of the prostate gland with MR spectroscopy offers the possibility for tumor-targeted radiation therapy (ie, intraprostatic dose escalation), which is applicable with both external radiation treatment and brachytherapy (51,52).

Conclusions

A combination of MR imaging and MR spectroscopy provides superb anatomic and metabolic images of prostate and pelvic anatomy, thus facilitating the detection of cancer and the evaluation of tumor volume, aggressiveness, and extent. With more refined techniques, more experienced readers, more uniform image interpretation, and greater emphasis on teamwork with members of the urology and radiation oncology departments, the MR imaging–MR spectroscopy approach will have tremendous potential to improve patient care.

References

1. American Cancer Society. Cancer facts and figures 2004. Publication No 5008.04. Atlanta, Ga: American Cancer Society, 2004.
2. Johansson JE, Holmberg L, Johansson S, Bergstrom R, Adami HO. Fifteen-year survival in prostate cancer: a prospective, population-based study in Sweden. JAMA 1997; 277:467–471.
3. Pound CR, Partin AW, Eisenberger MA, Chan DW, Pearson JD, Walsh PC. Natural history of progression after PSA elevation following radical prostatectomy. JAMA 1999; 281:1591–1597.
4. Physician Data Query (PDQ) of the National Cancer Institute: treatment options for health professionals—prostate cancer. Available at: *http://www.cancer.gov.* Accessed February 20, 2004.
5. Lu-Yao GL, Yao SL. Population-based study of long-term survival in patients with clinically localised prostate cancer. Lancet 1997; 349:906–910.
6. Holmberg L, Bill-Axelson A, Helgesen F, et al. A randomized trial comparing radical prostatectomy with watchful waiting in early prostate cancer. N Engl J Med 2002; 347:781–789.
7. Kattan MW, Eastham JA, Stapleton AM, Wheeler TM, Scardino PT. A preoperative nomogram for disease recurrence following radical prostatectomy for prostate cancer. J Natl Cancer Inst 1998; 90: 766–771.
8. Cookson MS, Fleshner NE, Soloway SM, Fair WR. Correlation between Gleason score of needle biopsy and radical prostatectomy specimen: accuracy and clinical implications. J Urol 1997; 157:559–562.
9. Coakley FV, Qayyum A, Kurhanewicz J. Magnetic resonance imaging and spectroscopic imaging of prostate cancer. J Urol 2003; 170:S69–S75; discussion S75–S76.
10. Barentsz JO, Engelbrecht M, Jager GJ, et al. Fast dynamic gadolinium-enhanced MR imaging of urinary bladder and prostate cancer. J Magn Reson Imaging 1999; 10:295–304.
11. Oyen RH. Dynamic contrast-enhanced MRI of the prostate: is this the way to proceed for characterization of prostatic carcinoma? Eur Radiol 2003; 13:921–924.
12. Ikonen S, Kivisaari L, Vehmas T, et al. Optimal timing of post-biopsy MR imaging of the prostate. Acta Radiol 2001; 42:70–73.
13. White S, Hricak H, Forstner R, et al. Prostate cancer: effect of postbiopsy hemorrhage on interpretation of MR images. Radiology 1995; 195:385–390.
14. Brown TR, Kincaid BM, Ugurbil K. NMR chemical shift imaging in three dimensions. Proc Natl Acad Sci U S A 1982; 79:3523–3526.
15. Star-Lack J, Nelson SJ, Kurhanewicz J, Huang LR, Vigneron DB. Improved water and lipid suppression for 3D PRESS CSI using RF band-selective inversion with gradient dephasing (BASING). Magn Reson Med 1997; 38:311–321.
16. McNeal JE. The zonal anatomy of the prostate. Prostate 1981; 2:35–49.
17. Engelbrecht MR, Huisman HJ, Laheij RJ, et al. Discrimination of prostate cancer from normal peripheral zone and central gland tissue by using dynamic contrast-enhanced MR imaging. Radiology 2003; 229:248–254.
18. Ogura K, Maekawa S, Okubo K, et al. Dynamic endorectal magnetic resonance imaging for local staging and detection of neurovascular bundle involvement of prostate cancer: correlation with histopathologic results. Urology 2001; 57:721–726.
19. Engelbrecht MR, Jager GJ, Laheij RJ, Verbeek AL, van Lier HJ, Barentsz JO. Local staging of prostate cancer using magnetic resonance imaging: a meta-analysis. Eur Radiol 2002; 12:2294–2302.
20. Kurhanewicz J, Vigneron DB, Hricak H, Narayan P, Carroll P, Nelson SJ. Three-dimensional 1H spectroscopic imaging of the in situ human prostate with high spatial (0.24 to 0.7 cm^3) spatial resolution. Radiology 1996; 198:795–805.
21. Males RG, Vigneron DB, Star-Lack J, et al. Clinical application of BASING and spectral/spatial water and lipid suppression pulses for prostate cancer staging and localization by in vivo 3D 1H magnetic resonance spectroscopic imaging. Magn Reson Med 2000; 43:17–22.
22. Scheidler J, Hricak H, Vigneron DB, et al. Prostate cancer: localization with three-dimensional proton MR spectroscopic imaging—clinicopathologic study. Radiology 1999; 213:473–480.
23. Sirovich BE, Schwartz LM, Woloshin S. Screening men for prostate and colorectal cancer in the United States: does practice reflect the evidence? JAMA 2003; 289:1414–1420.
24. Miller DC, Hafez KS, Stewart A, Montie JE, Wei JT. Prostate carcinoma presentation, diagnosis, and staging: an update from the National Cancer Data Base. Cancer 2003; 98:1169–1178.
25. Zakian KL, Eberhardt S, Hricak H, et al. Transition zone prostate cancer: metabolic characteristics at 1H MR spectroscopic imaging—initial results. Radiology 2003; 229:241–247.
26. Beyersdorff D, Taupitz M, Winkelmann B, et al. Patients with a history of elevated prostate-specific

antigen levels and negative transrectal US-guided quadrant or sextant biopsy results: value of MR imaging. Radiology 2002; 224:701–706.
27. Punglia RS, D'Amico AV, Catalona WJ, Roehl KA, Kuntz KM. Effect of verification bias on screening for prostate cancer by measurement of prostate-specific antigen. N Engl J Med 2003; 349:335–342.
28. Wefer AE, Hricak H, Vigneron DB, et al. Sextant localization of prostate cancer: comparison of sextant biopsy, magnetic resonance imaging and magnetic resonance spectroscopic imaging with step section histology. J Urol 2000; 164:400–404.
29. Rabbani F, Stroumbakis N, Kava BR, Cookson MS, Fair WR. Incidence and clinical significance of false-negative sextant prostate biopsies. J Urol 1998; 159:1247–1250.
30. Obek C, Louis P, Civantos F, Soloway MS. Comparison of digital rectal examination and biopsy results with the radical prostatectomy specimen. J Urol 1999; 161:494–498; discussion 498–499.
31. Steinberg DM, Sauvageot J, Piantadosi S, Epstein JI. Correlation of prostate needle biopsy and radical prostatectomy Gleason grade in academic and community settings. Am J Surg Pathol 1997; 21:566–576.
32. Zakian K, Sircar K, Hricak H, et al. Correlation of proton MR spectroscopic imaging with Gleason score based on step-section pathology after radical prostatectomy (abstr). Radiology 2002; 225(P):628.
33. Magnetic resonance imaging and magnetic resonance spectroscopic imaging in diagnosing the extent of disease in patients with prostate cancer (ACRIN-6659). Available at *http://www.cancer.gov/clinicaltrials.* Accessed April 28, 2004.
34. American Joint Committee on Cancer. Prostate. In: AJCC cancer staging manual. 6th ed. New York, NY: Springer, 2002; 309–316.
35. Hull GW, Rabbani F, Abbas F, Wheeler TM, Kattan MW, Scardino PT. Cancer control with radical prostatectomy alone in 1,000 consecutive patients. J Urol 2002; 167:528–534.
36. Catalona WJ, Ramos CG, Carvalhal GF. Contemporary results of anatomic radical prostatectomy. CA Cancer J Clin 1999; 49:282–296.
37. Harisinghani MG, Barentsz J, Hahn PF, et al. Noninvasive detection of clinically occult lymph-node metastases in prostate cancer. N Engl J Med 2003; 348:2491–2499.
38. Naya Y, Babaian RJ. The predictors of pelvic lymph node metastasis at radical retropubic prostatectomy. J Urol 2003; 170:2306–2310.
39. Wymenga LF, Boomsma JH, Groenier K, Piers DA, Mensink HJ. Routine bone scans in patients with prostate cancer related to serum prostate-specific antigen and alkaline phosphatase. BJU Int 2001; 88:226–230.
40. Coakley FV, Eberhardt S, Wei DC, et al. Blood loss during radical retropubic prostatectomy: relationship to morphologic features on preoperative endorectal magnetic resonance imaging. Urology 2002; 59:884–888.
41. Coakley FV, Eberhardt S, Kattan MW, Wei DC, Scardino PT, Hricak H. Urinary continence after radical retropubic prostatectomy: relationship with membranous urethral length on preoperative endorectal magnetic resonance imaging. J Urol 2002; 168:1032–1035.
42. Leibel SA, Fuks Z, Zelefsky MJ, et al. Intensity-modulated radiotherapy. Cancer J 2002; 8:164–176.
43. Pollack A, Hanlon A, Horwitz EM, Feigenberg S, Uzzo RG, Price RA. Radiation therapy dose escalation for prostate cancer: a rationale for IMRT. World J Urol 2003; 21:200–208.
44. Pollack A, Hanlon AL, Horwitz EM, Feigenberg SJ, Uzzo RG, Hanks GE. Prostate cancer radiotherapy dose response: an update of the Fox Chase experience. J Urol 2004; 171:1132–1136.
45. Kuban D, Pollack A, Huang E, et al. Hazards of dose escalation in prostate cancer radiotherapy. Int J Radiat Oncol Biol Phys 2003; 57:1260–1268.
46. Padhani AR, Nutting CM. Why do we need more accurate intraprostatic localization of cancer? Br J Radiol 2003; 76:585–586.
47. Roach M III, Faillace-Akazawa P, Malfatti C, Holland J, Hricak H. Prostate volumes defined by magnetic resonance imaging and computerized tomographic scans for three-dimensional conformal radiotherapy. Int J Radiat Oncol Biol Phys 1996; 35:1011–1018.
48. Debois M, Oyen R, Maes F, et al. The contribution of magnetic resonance imaging to the three-dimensional treatment planning of localized prostate cancer. Int J Radiat Oncol Biol Phys 1999; 45:857–865.
49. Rasch C, Barillot I, Remeijer P, Touw A, van Herk M, Lebesque JV. Definition of the prostate in CT and MRI: a multi-observer study. Int J Radiat Oncol Biol Phys 1999; 43:57–66.
50. Steenbakkers RJ, Deurloo KE, Nowak PJ, Lebesque JV, van Herk M, Rasch CR. Reduction of dose delivered to the rectum and bulb of the penis using MRI delineation for radiotherapy of the prostate. Int J Radiat Oncol Biol Phys 2003; 57:1269–1279.
51. Mizowaki T, Cohen GN, Fung AY, Zaider M. Towards integrating functional imaging in the treatment of prostate cancer with radiation: the registration of the MR spectroscopy imaging to ultrasound/CT images and its implementation in treatment planning. Int J Radiat Oncol Biol Phys 2002; 54:1558–1564.
52. DiBiase SJ, Hosseinzadeh K, Gullapalli RP, et al. Magnetic resonance spectroscopic imaging–guided brachytherapy for localized prostate cancer. Int J Radiat Oncol Biol Phys 2002; 52:429–438.

This article meets the criteria for 1.0 credit hour in category 1 of the AMA Physician's Recognition Award. To obtain credit, see accompanying test at http://www.rsna.org/education/rg_cme.html.